First constraints on fuzzy dark matter from Lyman-α forest data and hydrodynamical simulations

Vid Iršič[1,2,3],* Matteo Viel[4,5,6],† Martin G. Haehnelt [7], James S. Bolton [8], and George D. Becker[9,10]
[1] *University of Washington, Department of Astronomy, 3910 15th Ave NE, WA 98195-1580 Seattle, USA*
[2] *Institute for Advanced Study, 1 Einstein Drive, NJ 08540 Princeton, USA*
[3] *The Abdus Salam International Centre for Theoretical Physics, Strada Costiera 11, I-34151 Trieste, Italy*
[4] *SISSA-International School for Advanced Studies, Via Bonomea 265, 34136 Trieste, Italy*
[5] *INAF - Osservatorio Astronomico di Trieste, Via G. B. Tiepolo 11, I-34143 Trieste, Italy*
[6] *INFN - National Institute for Nuclear Physics, via Valerio 2, I-34127 Trieste, Italy*
[7] *Institute of Astronomy and Kavli Institute of Cosmology, Madingley Road, Cambridge CB3 0HA, UK*
[8] *School of Physics and Astronomy, University of Nottingham, University Park, Nottingham, NG7 2RD, UK*
[9] *Institute of Astronomy and Kavli Institute of Cosmology, Madingley Road, Cambridge CB3 0HA, UK*
[10] *Space Telescope Science Institute, 3700 San Martin Drive, Baltimore, MD 21218, USA*

We present constraints on the masses of extremely light bosons dubbed fuzzy dark matter from Lyman-α forest data. Extremely light bosons with a De Broglie wavelength of ~ 1 kpc have been suggested as dark matter candidates that may resolve some of the current small scale problems of the cold dark matter model. For the first time we use hydrodynamical simulations to model the Lyman-α flux power spectrum in these models and compare with the observed flux power spectrum from two different data sets: the XQ-100 and HIRES/MIKE quasar spectra samples. After marginalization over nuisance and physical parameters and with conservative assumptions for the thermal history of the IGM that allow for jumps in the temperature of up to 5000 K, XQ-100 provides a lower limit of 7.1×10^{-22} eV, HIRES/MIKE returns a stronger limit of 14.3×10^{-22} eV, while the combination of both data sets results in a limit of 20 $\times10^{-22}$ eV (2σ C.L.). The limits for the analysis of the combined data sets increases to 37.5×10^{-22} eV (2σ C.L.) when a smoother thermal history is assumed where the temperature of the IGM evolves as a power-law in redshift. Light boson masses in the range $1-10\times10^{-22}$ eV are ruled out at high significance by our analysis, casting strong doubts that FDM helps solve the "small scale crisis" of the cold dark matter models.

Introduction. Recently, there has been a growing interest in so-called Fuzzy Dark Matter (FDM) models where the dark matter is made of ultra-light bosons. Cosmological and astrophysical consequences have been comprehensively reviewed in [1–5] highlighting the particle physics motivation [6–9] for such models, as well as the importance of experimental searches [10]. A broad variety of astrophysical implications have been investigated in the literature: the halo mass function [11], the innermost structure of haloes [12–14], the dynamical properties of the smallest objects [15], the linear matter power spectrum [1], the development of non-linearities by using N-body simulations [16], the abundance of high redshift objects [17], the overall impact of FDM on galaxy formation and the reionization history of the Universe, the intergalactic medium [4, 18–21], pulsar timing and binary pulsars [22, 23], and the properties of our galactic disk [24]. The general conclusion is that in order to have an appreciable astrophysical impact the mass of ultra-light bosons would have to lie in the range $1-10\times10^{-22}$ eV, and in this mass range it is indeed possible that some small scale "tensions" of cold dark matter with observations could be alleviated (e.g. [25] for a review of the small scale "crisis" of cold dark matter).

The intergalactic medium (IGM) [26, 27] plays a unique role in constraining the (small scale) matter power spectrum, since the low-density, high redshift IGM filaments are particularly sensitive to the small scale properties of dark matter. The main observable manifestation of the IGM, the Lyman-α forest, has provided important constraints on the linear matter power spectrum, especially when combined with cosmic microwave background data [28–34]. This includes, most notably, the tightest constraints on warm dark matter (WDM) models [35–40], upper limits on neutrino masses [33, 40, 41] as well as the recent remarkable discovery of Baryonic

Acoustic Oscillations in the transmitted 3D flux [42, 43]. These results, especially those at small scales, are primarily due to the fact that the observed Lyman-α forest flux power spectrum provides a tracer of matter fluctuations on small scales and at high redshifts, where these fluctuations are still in the quasi-linear regime. At present, the tightest limits on the free streaming of WDM, expressed as the equivalent masses of thermal WDM relics, are in the range $m_{\rm WDM} > 2.3 - 5$ keV at 2σ C.L.. The values at the lower end of this range are probably overly conservative and require the assumption of thermal histories that are likely unphysical [44].

In FDM models, even though the typical de Broglie scale is rather small ($\sim$ kpc) the effect of FDM on the linear matter power spectrum is noticeable on scales larger than the smallest scales typically constrained by IGM data [1]. In the absence of fully numerical FDM simulations of the flux power spectrum, it has therefore become common practice to convert the limit on thermal relic WDM models – for which the flux power spectrum has been modelled in considerable detail – into FDM limits by comparing the linear matter power spectrum of WDM and FDM models and using the mass corresponding to $k_{1/2}$, the wavenumber at which the linear power spectrum departs (i.e. is suppressed) from the corresponding cold dark matter power spectrum by 50%. However, the accuracy of this rather crude mapping can only be checked by performing a full set of hydrodynamical simulations to model the effect of FDM on the properties of the IGM and the Lyman-α forest. Here, we will use such simulations to provide the first constraints on FDM models based on a full modelling of the Lyman-α flux power spectrum and comparison with two high-redshift data sets well suited to probing the small scale matter power spectrum. This will also allow us to check the accuracy of the $k_{1/2}$ mapping of thermal relic WDM constraints. Our analysis will be quite similar to the one presented in [36] and [45], where the flux power spectrum is modelled using a set of hydrodynamical simulations that vary astrophysical and cosmological parameters combined with a Monte Carlo Markov Chain analysis in the multi dimensional parameter space.

Data. The first sample we use is the set of 100 medium resolution, high signal-to-noise QSO spectra of the XQ-100 survey [46], with emission redshifts $3.5 < z < 4.5$. A more detailed description of the data and the power spectrum measurements of the XQ-100 survey can be found in [45]. Here we repeat the most important properties of the data and the derived flux power spectrum. The spectral resolution of the X-shooter spectrograph is 30-50 km/s, depending on wavelength. The flux power spectrum used in the analysis has been calculated for a total of 114 (k, z) data points in the ranges $z = 3, 3.2, 3.4, 3.6, 3.8, 4, 4.2$ and 19 bins in $k-$space in the range 0.003-0.057 s/km. We further use the measurements of the flux power spectrum presented in [36], at redshift bins $z = 4.2, 4.6, 5.0, 5.4$

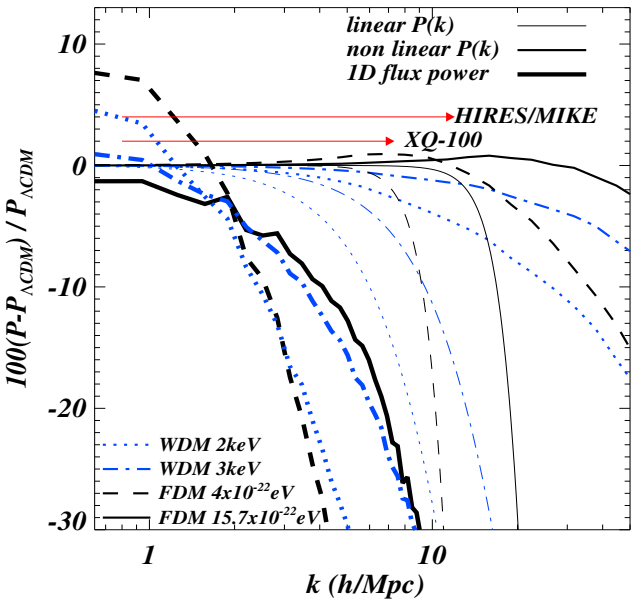

FIG. 1: Power spectrum relative to ΛCDM at $z = 5.4$ (in per cent). Linear matter, non-linear matter and flux power spectra are represented by the thin, thick and very thick curves, respectively. Black (blue) curves are for FDM (WDM) models with $m_{\rm FDM} = 5.7, 15.7 \times 10^{-22}$ eV ($m_{\rm WDM} = 2$, 3 keV).

and in 10 $k-$bins in the range 0.001-0.08 s/km. In this second sample the spectral resolution of the QSO absorption spectra obtained with the MIKE and HIRES spectrographs are about 13.6 and 6.7 km/s, respectively. As in the analysis of [36], a conservative cut is imposed on the flux power spectrum obtained from the MIKE and HIRES data, and only the measurements with $k > 0.005$ km^{-1} s are used to avoid possible systematic uncertainties on large scales due to continuum fitting.

Compared to XQ-100, the HIRES/MIKE sample has the advantage of probing smaller scales and higher redshift. There is a small redshift overlap between the two samples at $z = 4.2$. Since the thermal broadening (measured in km/s) of Lyman-α forest lines is roughly constant with redshift, the presence of a cutoff in the matter power spectrum due to free-streaming becomes more prominent in velocity space at high redshift due to the $H(z)/(1+z))$ scaling between the fixed comoving length scale set by the free-streaming length and the corresponding velocity scale. Moreover, the 1D power spectrum is more sensitive to the presence of a cutoff compared to the 3D power spectrum.

Simulations. Similarly as in [36] and [45], we model the flux power spectrum using a set of hydrodynamical simulations performed with the GADGET-3 code, a modified version of the publicly available Gadget-2 code [47]. A simplified star formation criterion is applied for which gas particles above an overdensity 1000, and below

T= 10^5 K are converted into stars (e.g. [48]). The reference model simulation has a box length of 20 Mpc/h with 2×768^3 and (cold) dark matter particles (gravitational softening of 1 comov. kpc/h) in a flat ΛCDM Universe with cosmological parameters $\Omega_{\rm m} = 0.301$, $\Omega_{\rm b} = 0.0457$, $n_{\rm s} = 0.961$, $H_0 = 70.2\,{\rm km\,s^{-1}\,Mpc^{-1}}$ and $\sigma_8 = 0.829$ in agreement with [49]. Three different WDM models with masses $m_{\rm WDM} = 2, 3, 4$ keV have also been simulated in order to obtain WDM constraints.

We simulate 5 different FDM models using the transfer function provided by [1] with light axion masses $\rm m_{FDM}$ of 1, 4, 5.7, 15.7 and 30 $\times 10^{-22}$ eV. These values have roughly the same $\rm k_{1/2}$ as models corresponding to thermal WDM relic masses of 1, 1.73, 2, 3, 3.87 keV, covering the range relevant for the "small scale crisis" of cold dark matter. These models were also simulated using the axionCAMB code [3] to obtain the linear transfer function, finding negligible impact on the simulated flux power. The corresponding ΛCDM model is also simulated along with a range of IGM thermal histories and cosmological parameters. In Fig. 1 we show the linear, non-linear and flux power spectrum at $z = 5.4$ for WDM and FDM models that have the same $\rm k_{1/2}$: non-linearities erase some of the information contained in the linear power spectrum. Note that the 1D flux power is much more sensitive to the cutoff. The maximum wavenumbers at which the flux power spectrum is measured by HIRES/MIKE and XQ-100 are represented by the horizontal arrows.

It has been noted before (e.g. [50]) that for the analysis of the Lyman-α it is sufficient to use the appropriate transfer function without modelling the full quantum effects below the de-Broglie wavelength of the FDM particle. This hypothesis is supported by the fact that the quantum pressure starts to dominate over gravity on scales smaller than the FDM Jeans scale ($k > k_J$) [50]. The FDM Jeans scale increases with cosmic time, and also increases with the mass of the FDM particle. For the largest redshift, $z = 5.4$, and smallest mass in our simulations, $m_{\rm FDM} = 1 \times 10^{-22}$ eV, the FDM Jeans scale is $64.7\,h\,{\rm Mpc^{-1}}$, which corresponds to scales smaller than the scale probed by our data ($k_{\rm max} = 12.7\,h\,{\rm Mpc^{-1}}$, for HIRES at $z = 5.4$). [1] The effect of quantum pressure term should thus have a negligible effect on the structure formation relevant for the Lyman-α forest.

We vary the thermal history by modifying the photo-heating rates in the simulations as in [51]. The low density IGM ($\Delta = 1 + \delta < 10$) is well described by a power-law temperature-density relation, $T = T_0 \Delta^{\gamma-1}$. We consider a range of values for the temperature at mean density T_0 and the slope of the $T-\rho$ relation, γ, based on the previous analysis of the Lyman-α forest and recent observations [52]. As in [45] these consist of a set of three different temperatures at mean density, $T_0(z = 3.6) = 7200, 11000, 14800$ K, which evolve with redshift, as well as a set of three values of the slope of the $T-\rho$ relation: $\gamma(z = 3.6) = 1.0, 1.3, 1.5$. The reference thermal history assumes $(T_0(z = 3.6), \gamma(z = 3.6)) = (11000\ {\rm K}, 1.5)$.

Following again [45] we use two parameters describing cosmology, σ_8 and $n_{\rm eff} = d \ln P_{\rm m}(k)/d \ln k$, evaluated at $k = 0.005\ {\rm km^{-1}\,s}$. Five different values are considered for both $\sigma_8 = 0.754, 0.804, 0.829, 0.854, 0.904$, and $n_{\rm eff} = -2.3474, -2.3274, -2.3074, -2.2874, -2.2674$. The reference model has $(\sigma_8, n_{\rm eff}, n_{\rm s}) = (0.829, -2.3074, 0.961)$. We also vary the redshift of reionization $z_{\rm rei}$ which is chosen to be $z_{\rm rei} = 9$ for the reference model as well as $z_{\rm rei} = 7, 15$ for two additional models [53]. The last parameter ($f_{\rm UV}$) characterizes the effect of Ultraviolet (UV) background fluctuations. An extreme model dominated by QSOs has been chosen with a strong scale dependence at higher redshift and towards large scales. The mean flux is also varied a-posteriori through rescaling the effective optical depth, $\tau_{\rm eff} = -\ln \bar{F}$. We use three different values $(0.8, 1, 1.2) \times \tau_{\rm obs,eff}$, with the observed value of $\tau_{\rm obs,eff}$ chosen to be those of the SDSS-III/BOSS measurements [54].

Method. Using the models of the flux obtained from the simulations we establish a grid of points for each redshift, in the parameter space of $(\bar{F}(z), T_0(z), \gamma(z), \sigma_8, z_{\rm rei}, n_{\rm eff}, f_{\rm UV}, m_{\rm FDM})$. We then perform a linear interpolation between the grid points in this multidimensional parameter space, to obtain predictions of flux power for the desired models. The interpolation is performed for $P_{\rm F}(k, z)$, directly, rather than for ratios of flux power w.r.t. the corresponding ΛCDM simulation as was done in [36]. Parameter constraints are then obtained with a Monte Carlo Markov Chain code that explores the likelihood space until convergence is reached.

The redshift evolution of the IGM parameters T_0 and γ are modelled as power-laws for our reference analysis: $T_0(z) = T_0^A \left[(1+z)/(1+z_{\rm p})\right]^{T_0^S}$ and $\gamma(z) = \gamma^A \left[(1+z)/(1+z_{\rm p})\right]^{\gamma^S}$. The pivot redshift is different for each data set and roughly corresponds to the redshift at which most of the data lies ($z_{\rm p} = 3.6, 4.5, 4.2$ for XQ-100, HIRES/MIKE and the combined analysis, respectively).

Results. In Figure 2 we show the main result of this letter: the marginalized 1D likelihood for $1/\rm m_{FDM}$. For our reference analysis, in which the temperature evolution is parameterized as a power-law at different pivot redshifts, XQ-100 returns an upper limit of 4.6×10^{-22} eV, HIRES/MIKE gives 16.4×10^{-22} eV, while the combination of the two data sets results in a considerable improvement to 37.5×10^{-22} eV (2σ C.L.). These numbers become 2.7, 16.5, 32.2 $\times 10^{-22}$ eV, for XQ-100,

[1] Furthermore, the growth rate ratio ξ, as defined in [50], is $\xi > 0.995$ for scales $k < 12.7\,h\,{\rm Mpc^{-1}}$ for the redshift range considered in this paper. The value of ξ decreases as we approach the FDM Jeans scale, with $\xi = 0.55$ at $k = 40\,h\,{\rm Mpc^{-1}}$.

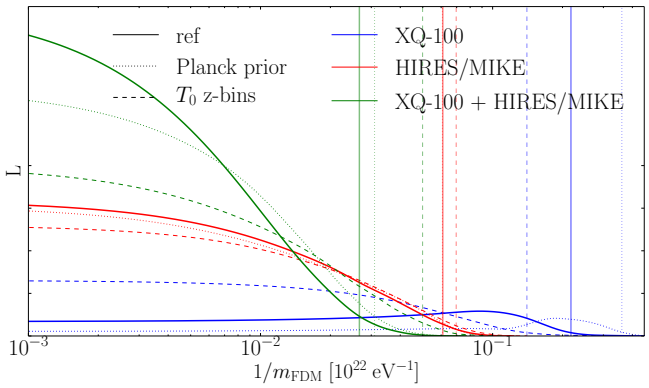

FIG. 2: 1D marginalized likelihood constraints for $1/m_{\rm FDM}$. XQ-100, HIRES/MIKE and XQ-100+HIRES/MIKE are represented by the blue, red and green curves, respectively, with (continuous curves) and without (dotted curves) using Planck priors. Additionally results for models where we vary temperature independently in each redshift bin are plotted as dashed curves. 2σ upper limits are represented by vertical lines.

$m_{\rm FDM}$ [10^{-22}eV]	XQ-100	HIRES/MIKE	Combined
ref.	4.5	16.4	37.5
Cov. × 1.3	3.9	16.3	34.9
Planck priors	2.7	16.5	32.2
$T_0(z)$ bins	7.1	14.3	20.0
$\chi^2/d.o.f.$ (ref.)	134/124	33/40	187/173

TABLE I: Marginalized constraints at 95 % (lower limits). The pivot redshifts for different data sets are: $z_{\rm p} = 3.6, 4.5, 4.2$ for XQ-100, HIRES/MIKE and combined for reference case, covariance matrix multiplied by 1.3, Planck priors and temperature in redshift bins.

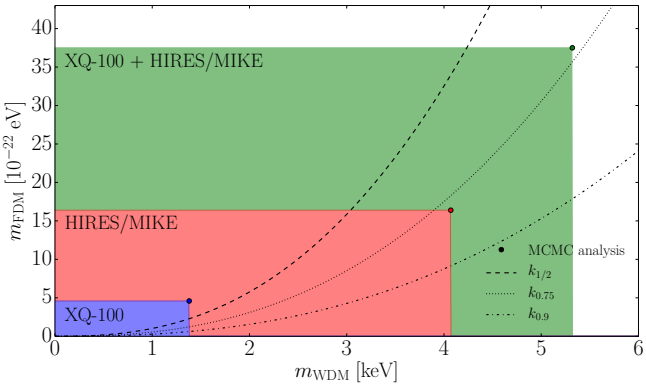

FIG. 3: Comparison of limits on $m_{\rm FDM}$ and $m_{\rm WDM}$ (thermal relic). Also shown is the relation obtained by matching $k_{1/2}$, $k_{0.75}$ and $k_{0.9}$ for the linear power spectra. Shaded areas show regions excluded by the analysis of XQ-100, HIRES/MIKE and both data sets in blue, red and green colors, respectively. Filled circles represent the 2σ C.L. lower limits for WDM and FDM.

HIRES/MIKE and both data sets, when using the following Planck priors on $n_{\rm eff} = -2.307 \pm 0.01$ and $\sigma_8 = 0.829 \pm 0.01$ (1σ Gaussian priors). The improvement in the joint constraints is due to the fact that when combining the two data sets the thermal evolution of the IGM is assumed to be one power-law for both $T_0(z)$ and $\gamma(z)$ for the full redshift range of the combined data sets. If we drop the assumption of a power-law evolution and we let the temperature vary independently in each redshift bin, with a maximum jump $\Delta T = 5000\,{\rm K}$ in bins that are separated by $\Delta z = 0.2$, we obtain 7.1, 14.3, 20.0 $\times 10^{-22}$ eV for XQ-100, HIRES/MIKE and both combined. We regard this result as the most conservative, since sudden jumps of temperature are not physically plausible in this redshift range (e.g. [55, 56]).

Increasing the covariance matrix by a multiplicative factor 1.3 in order to better represent a possible underestimation of the errors does not affect the results appreciably. In Tab. 1 we summarize the results including the $\chi^2/d.o.f.$ for the reference case, which appear to be very reasonable in all cases. For the combined analysis the other parameters lie within the following 2σ C.L. ranges at $z_{\rm p} = 4.2$: $\sigma_8 = [0.83, 0.95]$, $n_{\rm eff} = [-2.43, -2.31]$, $T^A(z_{\rm p})$ $[10^4\,{\rm K}] = [0.71, 1.06]$, $T^S(z_{\rm p}) = [-3.37, -0.80]$, $\gamma^A(z_{\rm p}) = [1.27, 1.69]$, $\gamma^S(z_{\rm p}) = [-0.11, 1.82]$, $z_{\rm rei} = [6.27, 13.62]$, $f_{\rm UV} = [0.04, 0.94]$.

We have verified the constraints obtained by considering additional simulations with $m_{\rm FDM}$ of 30 $\times 10^{-22}$ eV.

In Figure 3 we illustrate the relation between WDM and FDM constraints. Due to the lack of the detailed modelling of the flux power spectrum for FDM models using hydrodynamical simulation so far, it has been usually assumed that one can map thermal relic WDM masses into FDM constraints by identifying the corresponding $k_{1/2}$ values for the linear power spectra, i.e. the wavenumber at which the power reaches 50% of the ΛCDM linear power spectrum. Figure 3 shows that this is not a good approximation. For XQ-100 only, i.e. for a WDM constraint of 1.34 keV, the corresponding FDM limit is slightly above the $k_{1/2}$ curve, which remains a reasonable approximation. The HIRES/MIKE data only, however, gives a WDM lower limit of 4.7 keV that translates into a FDM limit which is much weaker than the one that would be obtained using the $k_{1/2}$ mapping. The same holds for the combined analysis. For these higher thermal relic WDM masses the WDM constraints are better mapped into FDM constrains by using $k_{0.75}$ rather than $k_{1/2}$, where $k_{0.75}$ is defined as the wavenumber at which the power reaches 75% of the ΛCDM linear power spectrum. The reason for this is that as the free-streaming cut-off moves to smaller scales for larger particle masses, the scales affected by the free-streaming cut-off become more non-linear.

We have also checked that similar conclusions are reached when considering the 1D linear power spectrum, which is the quantity really probed by the flux power spectrum (rather than the 3D power spectrum). The different data sets are obviously constraining linear power at different (k, z) values. Non-linearities will develop differently in WDM and FDM models and this makes the mapping between the two scenarios not straightforward. Full non-linear hydrodynamic simulations and detailed modelling of the flux power spectrum is required for accurate constraints on FDM models. WDM models retain more small scale power at $k > k_{0.75}$ compared to the corresponding FDM modelq that has instead a more prominent knee at $k < k_{0.75}$. These differences partially compensate in terms of non linear 1D flux power in a non-trivial way that depends on how non-linear the matter power spectrum is at the free-streaming scale. Similar to the shape of the WDM cutoff, the FDM cutoff in the flux power spectrum appears to be rather distinctive with no significant degeneracies with the other parameters in the analysis.

Conclusions. We have presented constraints on FDM models based on detailed modelling of the Lyman-α forest 1D flux power spectrum and high resolution data at intermediate and high redshifts with hydrodynamical simulations. These are the first constraints that incorporate the effect of the relevant IGM physics, including thermal and pressure smoothing on the non-linear evolution of the flux power spectrum on the relevant scales. Our final, conservative lower limit from a joint analysis of the intermediate and high-resolution Lyman-α forest data, $\mathrm{m_{FDM}} > 20 \times 10^{-22}$ eV (2σ C.L.), was obtained with conservative assumptions for the thermal history of the IGM that allow for (unphysical) sudden jumps of the IGM temperature up to 5000K. This lower limit for the mass of ultra-light bosons strengthens by about a further factor two if we assume a smoother thermal history of the IGM. Our analysis appears to close the window of FDM models with significant astrophysical implications, in particular for alleviating the tension between observations and theoretical predictions of cold dark matter models on small scales. [2]

VI is supported by US NSF grant AST-1514734. VI also thanks M. McQuinn for useful discussions, and IAS, Princeton, for hospitality during his stay where part of this work was completed. MV is supported by INFN/PD51 Indark and by the ERC Grant 257670-cosmoIGM and by PRIN-INAF "2012 "The X-Shooter sample of 100 quasar spectra at $z \sim 3.5$". JSB is supported by a Royal Society URF. MGH is supported by the FP7 ERC Grant Emergence-320596 and the Kavli Foundation. GB is supported by the NSF under award AST-1615814. Simulations were performed at the University of Cambridge with Darwin-HPCS and COSMOS, operated on behalf of the STFC DiRAC facility (funded by BIS National E-infrastructure capital grant ST/J005673/1 and STFC grants ST/H008586/1, ST/K00333X/1).

[2] After this paper was completed an analysis of IGM data has been performed by [57] reaching similar conclusions with slightly weaker constraints on FDM mass.

Supplemental material

The effect of pressure smoothing

The gas physics imprints two distinct scales on the distribution of the flux. The first is the thermal Doppler broadening, which smoothes the optical depth along the line of sight and this effect depends on the temperature at a given redshift. The second effect is from Jeans thermal pressure smoothing which affects the gas distribution relative to the 3D dark matter distribution. Because it takes some time for the gas to respond to the changes in temperature, this effect depends on the thermal history evolution at earlier times.

Similarly to pressure smoothing, additional smoothing due to FDM model also affects the 3D distribution. Thus a certain degree of degeneracy is expected.

In the analysis presented in this paper we have parametrised the effects of thermal physics by three main observables (T_0,γ and $z_{\rm rei}$), with further parameterisation of the redshift evolution of T_0 and γ (see main text for details). The pressure smoothing scale would thus mostly differ from the Doppler broadening scale due to the value of the redshift of reionisation ($z_{\rm rei}$).

Due to the different manifestation of the smoothing (1D vs 3D) between the thermal parameters, as well as different redshift evolution between thermal smoothing scales and FDM smoothing scale, degeneracies in the parameter space can be broken. This is shown in Fig. 4. The left hand panel shows that the temperature (T_0 at a chosen redshift) is degenerate with the FDM particle mass, particularly when estimating the parameters in the lower redshift range (blue contours - XQ-100 data set). The degeneracy is broken efficiently when moving to higher redshift range (red contours - HIRES/MIKE data) and almost gone when including all the data (green contours).

Moreover, the right hand side of Fig. 4 shows the degeneracy between the $m_{\rm FDM}$ and $z_{\rm rei}$ parameters. It is clear that when performing the analysis on higher redshift data, and increasing the redshift range, the degeneracy between these two parameters is almost broken. This indicates the importance of the different redshift evolution of the smoothing scales, for estimating the parameter values.

To further support this, we have estimated the thermal

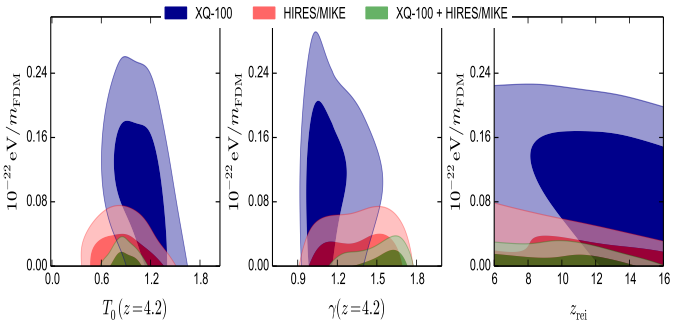

FIG. 4: The 2D contours between the thermal parameters and the FDM mass. Different colour schemes represent analysis obtained using XQ-100 only data set (blue contours), HIRES/MIKE (red contours) and finally XQ-100 and HIRES/MIKE data sets combined (green contours).

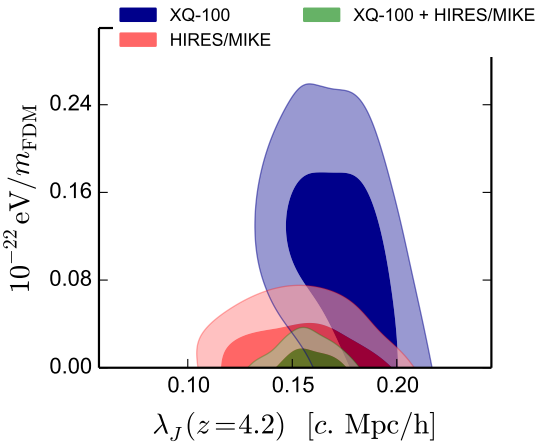

FIG. 5: The figure shows the 2D contours between m_{FDM} (governing FDM model smoothing) and the Jeans smoothing scale. The colour schemes reflect different data sets used in the analysis - XQ-100 only (blue), HIRES/MIKE (red) and combined data sets (green). The extent of smoothing increases with increasing values of both axis, i.e. larger value of $1/m_{\mathrm{FDM}}$ implies more smoothing due to FDM model, while larger value of λ_J implies more thermal smoothing.

Jeans pressure scale following [58]. As was shown in [58], the pressure smoothing scale (in Mpc/h) will always be smaller than the instantaneous Jeans scale. Moreover, a more recent analysis on the simulations has shown that the true pressure smoothing scale (at redshift concerning the Lyman-α forest) lies somewhere between the filtering and Jeans smoothing scale [59].

As was already discussed, the degeneracy between z_{rei} and m_{FDM} is very small, thus the expected difference between degeneracies in m_{FDM} vs λ_J plane will be small. This is illustrated in Fig. 5. The figure further shows (in the plane of the smoothing scales) that while degeneracy exists - either there is more thermal smoothing and less FDM smoothing or viceversa - it is severely broken when using higher redshift data, and when extending the redshift range of the analysis considered.

The best-fit FDM model

The Fig. 6 shows the data sets used in the analysis along with the best-fit model of the power-spectrum, when performing the analysis on the combined data set using the REF prior model. For comparison the plot also shows the power spectrum where the parameters were kept fixed at best-fit values, except the FDM particle mass was decreased down to 10×10^{-22}eV to guide the eye. The plot nicely illustrates that the shape of the cut-off is the most constraining effect when considering FDM models.

* E-mail: irsic@uw.edu (VI)
† E-mail: viel@sissa.it (MV)

[1] W. Hu, R. Barkana, and A. Gruzinov. Fuzzy Cold Dark Matter: The Wave Properties of Ultralight Particles. *Physical Review Letters*, 85:1158–1161, August 2000. doi: 10.1103/PhysRevLett.85.1158.

[2] T. Matos, F. S. Guzmán, and L. A. Ureña-López. Scalar field as dark matter in the universe. *Classical and Quantum Gravity*, 17:1707–1712, April 2000. doi: 10.1088/0264-9381/17/7/309.

[3] R. Hlozek, D. Grin, D. J. E. Marsh, and P. G. Ferreira. A search for ultralight axions using precision cosmological data. *Phys. Rev. D* , 91(10):103512, May 2015. doi: 10.1103/PhysRevD.91.103512.

[4] L. Hui, J. P. Ostriker, S. Tremaine, and E. Witten. On the hypothesis that cosmological dark matter is composed of ultra-light bosons. *ArXiv e-prints*, October

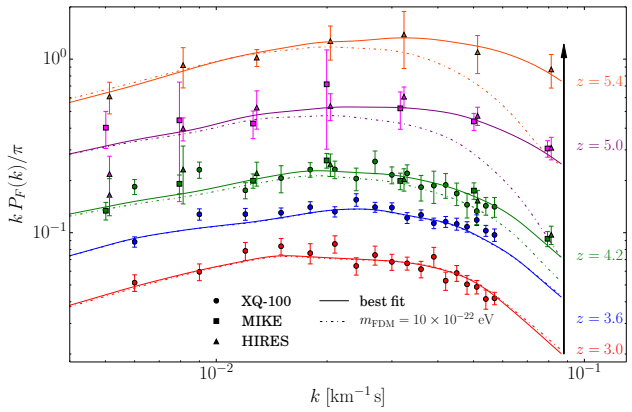

FIG. 6: The figure shows best-fit flux power spectrum obtained with analysis on the combined data sets (XQ-100 - circles, MIKE - squares and HIRES - triangles) using the REF prior model (see main text for detail). Different colours represent different redshifts, that are indicated on the right hand side of the plot, ranging from $z = 3$ to $z = 5.4$. The dashed lines show the flux power spectrum when all the parameters were kept at their best-fit values, except the mass of the FDM particle was decreased to 10×10^{-22}eV.

2016.

[5] T. Bernal, L. M. Fernández-Hernández, T. Matos, and M. A. Rodríguez-Meza. Rotation Curves of High-Resolution LSB and SPARC Galaxies in Wave (Fuzzy) and Multistate (Ultra-light Boson) Scalar Field Dark Matter. *ArXiv e-prints*, January 2017.

[6] M. R. Baldeschi, G. B. Gelmini, and R. Ruffini. On massive fermions and bosons in galactic halos. *Physics Letters B*, 122:221–224, March 1983. doi: 10.1016/0370-2693(83)90688-3.

[7] J. Preskill, M. B. Wise, and F. Wilczek. Cosmology of the invisible axion. *Physics Letters B*, 120:127–132, January 1983. doi: 10.1016/0370-2693(83)90637-8.

[8] P. Sikivie and Q. Yang. Bose-Einstein Condensation of Dark Matter Axions. *Physical Review Letters*, 103(11): 111301, September 2009. doi: 10.1103/PhysRevLett.103.111301.

[9] U.-H. Zhang and T. Chiueh. Evolution of linear wave dark matter perturbations in the radiation-dominant era. *ArXiv e-prints*, February 2017.

[10] P. Sikivie. Experimental tests of the 'invisible' axion. *Physical Review Letters*, 51:1415–1417, October 1983. doi: 10.1103/PhysRevLett.51.1415.

[11] D. J. E. Marsh and J. Silk. A model for halo formation with axion mixed dark matter. MNRAS, 437:2652–2663, January 2014. doi: 10.1093/mnras/stt2079.

[12] J.-W. Lee and I.-G. Koh. Galactic halos as boson stars. *Phys. Rev. D* , 53:2236–2239, February 1996. doi: 10.1103/PhysRevD.53.2236.

[13] F. S. Guzmán, T. Matos, and H. B. Villegas. Scalar fields as dark matter in spiral galaxies: comparison with experiments. *Astronomische Nachrichten*, 320:97, 1999.

[14] J. Zhang, Y.-L. Sming Tsai, K. Cheung, and M.-C. Chu. Ultra-Light Axion Dark Matter and its impacts on dark halo structure in N-body simulation. *ArXiv e-prints*, November 2016.

[15] E. Calabrese and D. N. Spergel. Ultra-light dark matter in ultra-faint dwarf galaxies. MNRAS, 460:4397–4402, August 2016. doi: 10.1093/mnras/stw1256.

[16] H.-Y. Schive, T. Chiueh, and T. Broadhurst. Cosmic structure as the quantum interference of a coherent dark wave. *Nature Physics*, 10:496–499, July 2014. doi: 10.1038/nphys2996.

[17] N. Menci, A. Merle, M. Totzauer, A. Schneider, A. Grazian, M. Castellano, and N. G. Sanchez. Fundamental physics with the Hubble Frontier Fields: constraining Dark Matter models with the abundance of extremely faint and distant galaxies. *ArXiv e-prints*, January 2017.

[18] L. Amendola and R. Barbieri. Dark matter from an ultra-light pseudo-Goldsone-boson. *Physics Letters B*, 642:192–196, November 2006. doi: 10.1016/j.physletb.2006.08.069.

[19] J. E. Kim and D. J. E. Marsh. An ultralight pseudoscalar boson. *Phys. Rev. D* , 93(2):025027, January 2016. doi: 10.1103/PhysRevD.93.025027.

[20] D. J. E. Marsh. Axion cosmology. *Physics Reports*, 643: 1–79, July 2016. doi: 10.1016/j.physrep.2016.06.005.

[21] A. Sarkar, S. K. Sethi, and S. Das. The effects of the small-scale behaviour of dark matter power spectrum on CMB spectral distortion. *ArXiv e-prints*, January 2017.

[22] D. Blas, D. Lopez Nacir, and S. Sibiryakov. Ultra-Light Dark Matter Resonates with Binary Pulsars. *ArXiv e-prints*, December 2016.

[23] A. Khmelnitsky and V. Rubakov. Pulsar timing signal from ultralight scalar dark matter. J. Cosmology Astropart. Phys., 2:019, February 2014. doi: 10.1088/1475-7516/2014/02/019.

[24] N. Banik, A. J. Christopherson, P. Sikivie, and E. M. Todarello. New astrophysical bounds on ultralight axionlike particles (ULALPs). *ArXiv e-prints*, January 2017.

[25] D. H. Weinberg, J. S. Bullock, F. Governato, R. Kuzio de Naray, and A. H. G. Peter. Cold dark matter: Controversies on small scales. *Proceedings of the National Academy of Science*, 112:12249–12255, October 2015. doi: 10.1073/pnas.1308716112.

[26] A. A. Meiksin. The physics of the intergalactic medium. *Reviews of Modern Physics*, 81:1405–1469, October 2009. doi: 10.1103/RevModPhys.81.1405.

[27] M. McQuinn. The Evolution of the Intergalactic Medium. *ArXiv e-prints*, November 2015.

[28] R. A. C. Croft, D. H. Weinberg, M. Bolte, S. Burles, L. Hernquist, N. Katz, D. Kirkman, and D. Tytler. Toward a Precise Measurement of Matter Clustering: Lyα Forest Data at Redshifts 2-4. *Astrophys. J.* , 581:20–52, December 2002. doi: 10.1086/344099.

[29] M. Zaldarriaga, R. Scoccimarro, and L. Hui. Inferring the Linear Power Spectrum from the Lyα Forest. *Astrophys. J.* , 590:1–7, June 2003. doi: 10.1086/374407.

[30] P. McDonald. Toward a Measurement of the Cosmological Geometry at z ˜ 2: Predicting Lyα Forest Correlation in Three Dimensions and the Potential of Future Data Sets. *Astrophys. J.* , 585:34–51, March 2003. doi: 10.1086/345945.

[31] M. Viel, M. G. Haehnelt, and V. Springel. Inferring the dark matter power spectrum from the Lyman α forest in high-resolution QSO absorption spectra. MNRAS, 354: 684–694, November 2004. doi: 10.1111/j.1365-2966.2004.08224.x.

[32] P. McDonald, U. Seljak, R. Cen, D. Shih, D. H. Weinberg, S. Burles, D. P. Schneider, D. J. Schlegel, N. A. Bahcall, J. W. Briggs, J. Brinkmann, M. Fukugita, Ž. Ivezić, S. Kent, and D. E. Vanden Berk. The Linear Theory Power Spectrum from the Lyα Forest in the Sloan Digital Sky Survey. *Astrophys. J.* , 635:761–783, December 2005. doi: 10.1086/497563.

[33] U. Seljak, A. Slosar, and P. McDonald. Cosmological parameters from combining the Lyman-α forest with CMB, galaxy clustering and SN constraints. J. Cosmology Astropart. Phys., 10:014, October 2006. doi: 10.1088/1475-7516/2006/10/014.

[34] A. Lidz, C.-A. Faucher-Giguère, A. Dall'Aglio, M. McQuinn, C. Fechner, M. Zaldarriaga, L. Hernquist, and S. Dutta. A Measurement of Small-scale Structure in the 2.2-4.2 Lyα Forest. *Astrophys. J.* , 718:199–230, July 2010. doi: 10.1088/0004-637X/718/1/199.

[35] M. Viel, J. Lesgourgues, M. G. Haehnelt, S. Matarrese, and A. Riotto. Constraining warm dark matter candidates including sterile neutrinos and light gravitinos with WMAP and the Lyman-α forest. *Phys. Rev. D* , 71(6): 063534, March 2005. doi: 10.1103/PhysRevD.71.063534.

[36] M. Viel, G. D. Becker, J. S. Bolton, and M. G. Haehnelt. Warm dark matter as a solution to the small scale crisis: New constraints from high redshift Lyman-α forest data. *Phys. Rev. D* , 88(4):043502, August 2013. doi: 10.1103/PhysRevD.88.043502.

[37] U. Seljak, A. Makarov, P. McDonald, and H. Trac. Can Sterile Neutrinos Be the Dark Matter? *Physical Review Letters*, 97(19):191303, November 2006. doi: 10.1103/PhysRevLett.97.191303.

[38] J. Baur, N. Palanque-Delabrouille, C. Yèche, C. Magneville, and M. Viel. Lyman-alpha forests cool warm dark matter. J. Cosmology Astropart. Phys., 8:012, August 2016. doi: 10.1088/1475-7516/2016/08/012.

[39] M. Viel, G. D. Becker, J. S. Bolton, M. G. Haehnelt, M. Rauch, and W. L. W. Sargent. How Cold Is Cold Dark Matter? Small-Scales Constraints from the Flux Power Spectrum of the High-Redshift Lyman-α Forest. *Physical Review Letters*, 100(4):041304, February 2008. doi: 10.1103/PhysRevLett.100.041304.

[40] C. Yeche, N. Palanque-Delabrouille, J . Baur, and H. du Mas des BourBoux. Constraints on neutrino masses from Lyman-alpha forest power spectrum with BOSS and XQ-100. *ArXiv e-prints*, February 2017.

[41] N. Palanque-Delabrouille, C. Yèche, J. Baur, C. Magneville, G. Rossi, J. Lesgourgues, A. Borde, E. Burtin, J.-M. LeGoff, J. Rich, M. Viel, and D. Weinberg. Neutrino masses and cosmology with Lyman-alpha forest power spectrum. J. Cosmology Astropart. Phys., 11:011, November 2015. doi: 10.1088/1475-7516/2015/11/011.

[42] N. G. Busca, T. Delubac, J. Rich, S. Bailey, A. Font-Ribera, D. Kirkby, J.-M. Le Goff, M. M. Pieri, A. Slosar, É. Aubourg, J. E. Bautista, D. Bizyaev, M. Blomqvist, A. S. Bolton, J. Bovy, H. Brewington, A. Borde, J. Brinkmann, B. Carithers, R. A. C. Croft, K. S. Dawson, G. Ebelke, D. J. Eisenstein, J.-C. Hamilton, S. Ho, D. W. Hogg, K. Honscheid, K.-G. Lee, B. Lundgren, E. Malanushenko, V. Malanushenko, D. Margala, C. Maraston, K. Mehta, J. Miralda-Escudé, A. D. Myers, R. C. Nichol, P. Noterdaeme, M. D. Olmstead, D. Oravetz, N. Palanque-Delabrouille, K. Pan, I. Pâris, W. J. Percival, P. Petitjean, N. A. Roe, E. Rollinde, N. P. Ross, G. Rossi, D. J. Schlegel, D. P. Schneider, A. Shelden, E. S. Sheldon, A. Simmons, S. Snedden, J. L. Tinker, M. Viel, B. A. Weaver, D. H. Weinberg, M. White, C. Yèche, and D. G. York. Baryon acoustic oscillations in the Lyα forest of BOSS quasars. A&A, 552:A96, April 2013. doi: 10.1051/0004-6361/201220724.

[43] A. Slosar, V. Iršič, D. Kirkby, S. Bailey, N. G. Busca, T. Delubac, J. Rich, É. Aubourg, J. E. Bautista, V. Bhardwaj, M. Blomqvist, A. S. Bolton, J. Bovy, J. Brownstein, B. Carithers, R. A. C. Croft, K. S. Dawson, A. Font-Ribera, J.-M. Le Goff, S. Ho, K. Honscheid, K.-G. Lee, D. Margala, P. McDonald, B. Medolin, J. Miralda-Escudé, A. D. Myers, R. C. Nichol, P. Noterdaeme, N. Palanque-Delabrouille, I. Pâris, P. Petitjean, M. M. Pieri, Y. Piškur, N. A. Roe, N. P. Ross, G. Rossi, D. J. Schlegel, D. P. Schneider, N. Suzuki, E. S. Sheldon, U. Seljak, M. Viel, D. H. Weinberg, and C. Yèche. Measurement of baryon acoustic oscillations in the Lyman-α forest fluctuations in BOSS data release 9. J. Cosmology Astropart. Phys., 4:026, April 2013. doi: 10.1088/1475-7516/2013/04/026.

[44] A. Garzilli, A. Boyarsky, and O. Ruchayskiy. Cutoff in the Lyman {\alpha} forest power spectrum: warm IGM or warm dark matter? *ArXiv e-prints*, October 2015.

[45] V. Iršič, M. Viel, T. A. M. Berg, V. D'Odorico, M. G. Haehnelt, S. Cristiani, G. Cupani, T.-S. Kim, S. López, S. Ellison, G. D. Becker, L. Christensen, K. D. Denney, G. Worseck, and J. S. Bolton. The Lyman-alpha forest power spectrum from the XQ-100 Legacy Survey. MNRAS, December 2016. doi: 10.1093/mnras/stw3372.

[46] S. López, V. D'Odorico, S. L. Ellison, G. D. Becker, L. Christensen, G. Cupani, K. D. Denney, I. Pâris, G. Worseck, T. A. M. Berg, S. Cristiani, M. Dessauges-Zavadsky, M. Haehnelt, F. Hamann, J. Hennawi, V. Iršič, T.-S. Kim, P. López, R. Lund Saust, B. Ménard, S. Perrotta, J. X. Prochaska, R. Sánchez-Ramírez, M. Vestergaard, M. Viel, and L. Wisotzki. XQ-100: A legacy survey of one hundred $z = 3.5 - 4.5$ quasars observed with VLT/X-shooter. A&A, 594:A91, October 2016. doi: 10.1051/0004-6361/201628161.

[47] Volker Springel. The cosmological simulation code GADGET-2. MNRAS, 364:1105–1134, 2005. doi: 10.1111/j.1365-2966.2005.09655.x. URL `http://www.mpa-garching.mpg.de/gadget/`.

[48] J. S. Bolton, E. Puchwein, D. Sijacki, M. G. Haehnelt, T.-S. Kim, A. Meiksin, J. A. Regan, and M. Viel. The Sherwood simulation suite: overview and data comparisons with the Lyman-alpha forest at redshifts $2 < z < 5$. *ArXiv e-prints*, May 2016.

[49] Planck Collaboration, P. A. R. Ade, N. Aghanim, M. Arnaud, M. Ashdown, J. Aumont, C. Baccigalupi, A. J. Banday, R. B. Barreiro, J. G. Bartlett, and et al. Planck 2015 results. XIII. Cosmological parameters. A&A, 594:A13, September 2016. doi: 10.1051/0004-6361/201525830.

[50] H.-Y. Schive, T. Chiueh, T. Broadhurst, and K.-W. Huang. Contrasting Galaxy Formation from Quantum Wave Dark Matter, ψDM, with ΛCDM, using Planck and Hubble Data. *Astrophys. J.* , 818:89, February 2016. doi: 10.3847/0004-637X/818/1/89.

[51] J. S. Bolton, M. Viel, T.-S. Kim, M. G. Haehnelt, and R. F. Carswell. Possible evidence for an inverted temperature-density relation in the intergalactic medium from the flux distribution of the Lyα forest. MNRAS,

386:1131–1144, May 2008. doi: 10.1111/j.1365-2966.2008.13114.x.

[52] G. D. Becker, J. S. Bolton, M. G. Haehnelt, and W. L. W. Sargent. Detection of extended He II reionization in the temperature evolution of the intergalactic medium. MNRAS, 410:1096–1112, January 2011. doi: 10.1111/j.1365-2966.2010.17507.x.

[53] See Supplemental Material at [url] for a discussion on how the temperature and redshift of reionization affect the thermal Jeans smoothing, which includes [58, 59].

[54] N. Palanque-Delabrouille, C. Yèche, A. Borde, J.-M. Le Goff, G. Rossi, M. Viel, É. Aubourg, S. Bailey, J. Bautista, M. Blomqvist, A. Bolton, J. S. Bolton, N. G. Busca, B. Carithers, R. A. C. Croft, K. S. Dawson, T. Delubac, A. Font-Ribera, S. Ho, D. Kirkby, K.-G. Lee, D. Margala, J. Miralda-Escudé, D. Muna, A. D. Myers, P. Noterdaeme, I. Pâris, P. Petitjean, M. M. Pieri, J. Rich, E. Rollinde, N. P. Ross, D. J. Schlegel, D. P. Schneider, A. Slosar, and D. H. Weinberg. The one-dimensional Lyα forest power spectrum from BOSS. A&A, 559:A85, November 2013. doi: 10.1051/0004-6361/201322130.

[55] E. Puchwein, J. S. Bolton, M. G. Haehnelt, P. Madau, G. D. Becker, and F. Haardt. The photoheating of the intergalactic medium in synthesis models of the UV background. MNRAS, 450:4081–4097, July 2015. doi: 10.1093/mnras/stv773.

[56] P. R. Upton Sanderbeck, A. D'Aloisio, and M. J. McQuinn. Models of the thermal evolution of the intergalactic medium after reionization. MNRAS, 460:1885–1897, August 2016. doi: 10.1093/mnras/stw1117.

[57] E. Armengaud, N. Palanque-Delabrouille, C. Yèche, D. J. E. Marsh, and J. Baur. Constraining the mass of light bosonic dark matter using SDSS Lyman-α forest. *ArXiv e-prints*, March 2017.

[58] Nickolay Y. Gnedin and Lam Hui. Probing the universe with the Lyman alpha forest: 1. Hydrodynamics of the low density IGM. *Mon. Not. Roy. Astron. Soc.*, 296:44–55, 1998. doi: 10.1046/j.1365-8711.1998.01249.x.

[59] G. Kulkarni, J. F. Hennawi, J. Oñorbe, A. Rorai, and V. Springel. Characterizing the Pressure Smoothing Scale of the Intergalactic Medium. *Astrophys. J.* , 812:30, October 2015. doi: 10.1088/0004-637X/812/1/30.